

Triplet Electronic States in d^2 and d^8 Complexes Probed by Absorption Spectroscopy: A CASSCF/CASPT2 Analysis of $[\text{V}(\text{H}_2\text{O})_6]^{3+}$ and $[\text{Ni}(\text{H}_2\text{O})_6]^{2+}$

Julie Landry-Hum,[†] Guillaume Bussière,[†] Chantal Daniel,^{*,‡} and Christian Reber^{*,†}

Laboratoire de Chimie Quantique, UMR 7551 CNRS/Université Louis Pasteur, Institut Le Bel, 4 Rue Blaise Pascal, 67 000 Strasbourg, France, and Département de chimie, Université de Montréal, Montréal QC H3C 3J7, Canada

Received September 26, 2000

Octahedral complexes of transition metal ions with d^2 and d^8 electron configurations have triplet electronic states with identical T_{2g} , A_{2g} , $T_{1g}(^3F)$, and $T_{1g}(^3P)$ symmetry labels. CASSCF and CASPT2 calculations indicate the predominant electronic configurations for each triplet state. The two $^3T_{1g}$ states show strong configuration mixing in the d^8 complex $[\text{Ni}(\text{H}_2\text{O})_6]^{2+}$, but much weaker mixing occurs between these states in the d^2 compound $[\text{V}(\text{H}_2\text{O})_6]^{3+}$. Calculated vibrational frequencies and equilibrium geometries for the triplet states are used to obtain theoretical absorption spectra that are in agreement with the experimental data.

Introduction

Broad bands arising from spin-allowed $d-d$ transitions in the visible and near-infrared dominate the absorption spectra of many transition metal compounds. An excellent qualitative description of the electronic states involved in these transitions is obtained from crystal field theory for a complex in a "frozen" molecular configuration, excluding any vibronic processes. Potential energy surfaces are needed for a more complete description of the vibronic transitions, which always involve changes in the molecular structure.¹ These potential energy surfaces are traditionally determined from a Franck–Condon analysis of the experimental vibronic spectra. Particularly precise information can be obtained from spectra with resolved vibronic progressions.² Such empirical potential energy surfaces do not, in general, allow us to characterize electronic configurations or coupling between electronic states, and it is usually assumed that the electronic configuration obtained from the crystal field model for a single molecular geometry does not vary along the normal coordinates.

Optical absorption and luminescence spectra have been used to obtain experimental information on coupling effects between electronic states in specific situations. We have illustrated such effects for singlet and triplet states in $[\text{Ni}(\text{H}_2\text{O})_6]^{2+}$ ^{3,4} and related complexes of metal ions with a d^8 configuration, as well as for *trans*-dioxo complexes of rhenium(V) and osmium(VI) complexes, metal centers with a d^2 configuration.⁵ In the nickel(II) complexes, unusual progressions appear in the absorption spectrum due to a crossing between the lowest energy singlet

state and a triplet excited state. The luminescence spectra of the rhenium and osmium complexes show vibronic structure that reveals coupling effects between the singlet ground state and several excited states. The coupling in all these complexes involves states with different spin multiplicity, and its effects can be analyzed from experimental spectra with resolved vibronic structure.

In this paper, we investigate interactions between states with identical spin multiplicity that lead to absorption bands without resolved structure. For our model study, we choose the low energy triplet excited states of $[\text{Ni}(\text{H}_2\text{O})_6]^{2+}$ and of $[\text{V}(\text{H}_2\text{O})_6]^{3+}$. These states arise from different electronic configurations, and we compare our quantitative results to the expectations from crystal field theory. We present potential energy curves (PEC) based on CASSCF and CASPT2 calculations and focus on the contributions of different electronic configurations for the two $^3T_{1g}$ states along the single normal coordinate used in our model. Absorption spectra calculated from these potential curves involve no adjustable parameters, and we compare calculated band maxima, bandwidths, and vibrational frequencies to the experimental spectra. We take advantage of the electron–hole analogy to illustrate the interacting $^3T_{1g}$ states for the d^2 and d^8 electronic configurations and to explore the vibronic spectra that can be expected from these coupled states. The ground-state properties of the title compounds and many other aquo complexes have been explored by detailed electronic structure calculations,⁶ but effects involving coupled excited states have not been investigated.

Six-coordinate nickel(II) centers doped into halide lattices show absorption spectra similar to $[\text{Ni}(\text{H}_2\text{O})_6]^{2+}$. These solid materials have unusual spectroscopic properties, such as luminescence from higher energy excited states, allowing for the observation of intriguing optical effects.^{7–12} A very important

[†] Université de Montréal.

[‡] CNRS/Université Louis Pasteur.

- (1) Zink, J. I.; Kim Shin, K.-S. In *Advances in Photochemistry*; Volman, D. H., Hammond, G. S., Neckers, D. C., Eds.; John Wiley: New York, 1991; Vol. 16, p 119.
- (2) Brunold, T.; Güdel, H. U. In *Inorganic Electronic Structure and Spectroscopy*; Solomon, E. I., Lever, A. B. P., Eds.; John Wiley: New York, 1999; p 259.
- (3) Bussière, G.; Reber, C. *J. Am. Chem. Soc.* **1998**, *120*, 6306.
- (4) Triest, M.; Bussière, G.; Bélisle, H.; Reber, C. *J. Chem. Educ.* **2000**, *77*, 670. Full article: <http://jchemed.chem.wisc.edu/JCEWWW/Articles/index.html>.
- (5) Savoie, C.; Reber, C. *J. Am. Chem. Soc.* **2000**, *122*, 844.

- (6) Åkesson, R.; Pettersson, L. G. M.; Sandström, M.; Wahlgren, U. *J. Am. Chem. Soc.* **1994**, *116*, 8691.
- (7) Oetliker, U.; Riley, M. J.; Güdel, H. U. *J. Lumin.* **1995**, *63*, 63–73.
- (8) Oetliker, U.; Riley, M. J.; May, P. S.; Güdel, H. U. *J. Lumin.* **1992**, *53*, 553–556.
- (9) Oetliker, U.; Reber, C. *Phys. Chem. Commun.* **1999**, article 13.
- (10) Hehlen, M.; Güdel, H. U. *J. Chem. Phys.* **1992**, *98*, 1768.
- (11) May, P. S.; Güdel, H. U. *Chem. Phys. Lett.* **1989**, *164*, 612.

factor leading to these properties is the large energy separation between the two ${}^3T_{1g}$ states, to which the states mixing contributes, as discussed in the following for our two model complexes. Our calculations rationalize this energy separation and underline the importance of mixing between electronic states of transition metal chromophores.

Experimental Section and Spectroscopic Results

$[\text{Ni}(\text{H}_2\text{O})_6]^{2+}$ was crystallized as the Tutton salt $(\text{NH}_4)_2\text{Ni}(\text{SO}_4)_2 \cdot 6\text{H}_2\text{O}$ from H_2O and D_2O , respectively, and an aqueous solution of $[\text{V}(\text{H}_2\text{O})_6]^{3+}$ was prepared from $\text{VCl}_3 \cdot 6\text{H}_2\text{O}$ dissolved in 2 M H_2SO_4 . Absorption spectra were measured on a Varian Cary5E spectrometer, and Raman spectra were obtained with a Renishaw System 3000 spectrometer using the 514.5 nm line of an Ar⁺ ion laser as excitation source.

The spin-allowed transitions to triplet crystal field excited states are easily observed in near-infrared and visible absorption spectra of the two title complexes and have been reported in the literature.^{3,4,13–16} Our spectra of $[\text{V}(\text{H}_2\text{O})_6]^{3+}$ are identical to those in the literature.^{13–15,17} The triplet crystal field bands of both $[\text{Ni}(\text{H}_2\text{O})_6]^{2+}$ and $[\text{V}(\text{H}_2\text{O})_6]^{3+}$ do not show resolved vibronic structure at room temperature. In contrast, the lowest energy band of $[\text{Ni}(\text{H}_2\text{O})_6]^{2+}$ crystallized, as the Tutton salt shows well-resolved structure for both the H_2O and D_2O ligands at low temperature. To the best of our knowledge, resolved spectra for this transition have not been reported before for $[\text{Ni}(\text{H}_2\text{O})_6]^{2+}$.

Figure 1a shows the solution absorption spectra of $[\text{Ni}(\text{D}_2\text{O})_6]^{2+}$ and $[\text{V}(\text{H}_2\text{O})_6]^{3+}$, and the assignments of their spin-allowed bands are given in idealized O_h symmetry, used for simplicity throughout the following. We dissolved the nickel complex in D_2O in order to obtain a better spectrum in the region of the onset to the lowest energy triplet band, where vibrational overtones of H_2O mask the crystal field transition. The band maxima observed in solution do not vary significantly between $[\text{Ni}(\text{H}_2\text{O})_6]^{2+}$ and $[\text{Ni}(\text{D}_2\text{O})_6]^{2+}$ for the level of detail shown in Figure 1a. The transition to the ${}^3A_{2g}$ excited state of $[\text{V}(\text{H}_2\text{O})_6]^{3+}$ cannot be unambiguously identified from the literature spectra and from our own measurements, and it is therefore not included in our discussion.

Low-temperature spectra in the energy region of the onset of the lowest energy absorption band are given in Figure 1b for the crystalline $[\text{Ni}(\text{H}_2\text{O})_6]^{2+}$ and $[\text{Ni}(\text{D}_2\text{O})_6]^{2+}$ complexes. The crystals have well-defined extinction directions, but the relative intensities of the resolved transitions do not show distinct polarization effects. We therefore report unpolarized spectra obtained on approximately 3 mm thick crystals in Figure 1b. The spectra show resolved vibronic structure, in contrast to the higher energy spin-allowed bands of $[\text{Ni}(\text{H}_2\text{O})_6]^{2+}$ and to all spin-allowed transitions of $[\text{V}(\text{H}_2\text{O})_6]^{3+}$, where the resolution of the spectra is significantly inferior to Figure 1b.

The well-resolved peaks in Figure 1b correspond to transitions to the individual components of the ${}^3T_{2g}$ state, which is split by spin-orbit coupling and the low site symmetry of the complex in the crystal.¹⁸ It is important to note that both spectra in Figure 1b show distinct progressions with an interval of approximately 350 cm^{-1} . This frequency corresponds to the totally symmetric Ni–H₂O stretching mode observed at 397 cm^{-1} in the Raman spectrum at 77 K. The low-temperature spectrum shows barely resolved shoulders separated by 350 cm^{-1} across the band, and progressions in this mode have been reported for the ${}^3T_{1g}({}^3F)$ excited state in a detailed study of $[\text{Ni}(\text{H}_2\text{O})_6]^{2+}$ in a series of crystal lattices.¹⁶ This is therefore the most important mode determining the overall bandwidth. The spectrum is much less resolved at energies higher than the wavenumber range shown in Figure 1b, making it impossible to observe and analyze long progressions and

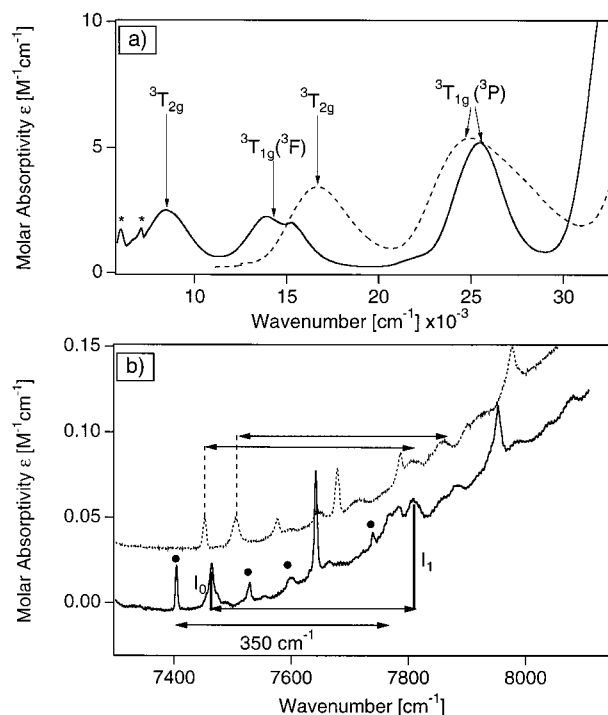


Figure 1. (a) Visible and near-infrared solution absorption spectra of $[\text{Ni}(\text{D}_2\text{O})_6]^{2+}$ (solid line) and $[\text{V}(\text{H}_2\text{O})_6]^{3+}$ (broken line) at room temperature with the assignment for all spin-allowed crystal field bands. The asterisks in the spectrum of $[\text{Ni}(\text{D}_2\text{O})_6]^{2+}$ denote vibrational overtones or instrumental artifacts. (b) Single-crystal absorption spectra of crystalline $(\text{NH}_4)_2\text{Ni}(\text{SO}_4)_2 \cdot 6(\text{H}_2\text{O})$ (solid line) and its deuterated analogue (dotted line, offset along the ordinate for clarity) at 5 K in the origin region of the lowest energy electronic transition. The dots denote transitions separated by equal energy intervals in the hydrated and deuterated complexes.

even to observe the first member of the 350 cm^{-1} progression on some of the higher energy vibronic origins. Weaker progressions in a mode with a frequency of approximately 200 cm^{-1} are also observed. They probably correspond to one of the Jahn–Teller active e_g and t_{2g} modes in the idealized O_h symmetry. These modes have frequencies of 299 and 232 cm^{-1} in the ground state, as determined from the Raman spectra at 77 K.

The comparison between the spectra of $[\text{Ni}(\text{H}_2\text{O})_6]^{2+}$ and $[\text{Ni}(\text{D}_2\text{O})_6]^{2+}$ in Figure 1b allows us to identify vibronic transitions. The difference between the lowest energy peak and higher energy resolved transitions is systematically lowered for vibronic transitions of the deuterated complex. This comparison indicates that the transition at 7464 cm^{-1} denoted as l_0 on the lower trace of Figure 1b and the intense bands observed at 7642 and 7954 cm^{-1} for $[\text{Ni}(\text{H}_2\text{O})_6]^{2+}$ are vibronic origins. The bands whose energy difference from the lowest energy transition does not change with deuteration are marked with dots in Figure 1b. It is tempting to assign these four bands as the electronic origins of transitions to the four spin-orbit components E_g , T_{1g} , T_{2g} , and A_{2g} expected in O_h symmetry, as the NiO_6 fragment of the complex does not deviate significantly from O_h symmetry.¹⁸ These spin-orbit levels cover an energy range of approximately 600 cm^{-1} for crystal field parameters that reproduce all spin allowed d–d bands and the lowest energy spin forbidden transition. The ground-state spin-orbit coupling constant λ of -270 cm^{-1} was used for the calculations.^{3,19,20} The bands marked with dots in Figure 1b span a range of approximately 300 cm^{-1} . This reduction is possibly a consequence of a Ham effect, in analogy to the corresponding lowest energy $t_{2g} \rightarrow e_g$ excitation studied

(12) May, P. S.; Güdel, H. U. *J. Lumin.* **1990**, *47*, 19.

(13) McClure, D. S. *Solid State Phys.* **1959**, *8/9*, 1.

(14) Hitchman, M. A.; McDonald, R. G.; Smith, P. W.; Stranger, R. J. *Chem. Soc., Dalton Trans.* **1988**, 1393.

(15) Tregenna-Piggott, P. W. L.; Best, S. P.; Güdel, H. U.; Weihe, H.; Wilson, C. C. *J. Solid State Chem.* **1999**, *145*, 460.

(16) Solomon, E. I.; Ballhausen, C. J. *Mol. Phys.* **1975**, *29*, 279.

(17) Johnson, D. A.; Nelson, P. G. *Inorg. Chem.* **1999**, *38*, 4949.

(18) Grimes, N. W.; Kay, H. F.; Webb, M. W. *Acta Crystallogr.* **1963**, *16*, 823.

(19) Liehr, A. D.; Ballhausen, C. J. *Ann. Phys.* **1959**, *2*, 134.

(20) The following crystal field parameters were used: $Dq = 910 \text{ cm}^{-1}$, $B = 950 \text{ cm}^{-1}$, $C/B = 4$, $\lambda = -270 \text{ cm}^{-1}$. The ${}^3T_{2g}$ energies calculated with these values are as follows: 8872 cm^{-1} (E_g), 8995 cm^{-1} (T_{1g}), 9315 cm^{-1} (T_{2g}), 9451 cm^{-1} (A_{2g}).

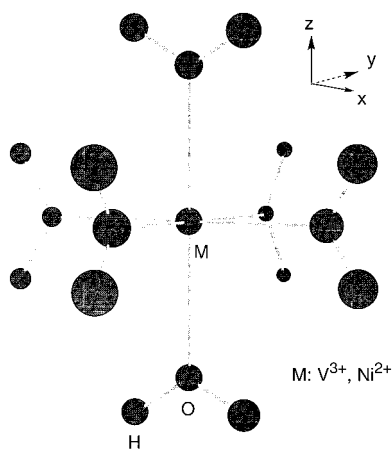


Figure 2. Molecular structure and coordinate system used for the CASSCF/CASPT2 calculations.

in detail for a number of chromium(III) complexes.^{21,22} We do not attempt to quantitatively analyze this splitting pattern due to the lack of information on electronic origins that could be hidden in the higher-energy region of the band, which shows significantly less resolution than the wavenumber range shown in Figure 1b. Large splittings of the ${}^3\text{T}_{2g}$ state cannot be ruled out for the title complexes due to the influence of anisotropic π bonding, which depends strongly on the position of the hydrogen atoms in each water ligand. This effect is not explored in the model calculations discussed in the following.

Computational Methods

The molecular structures of $[\text{M}(\text{H}_2\text{O})_6]^{n+}$ ($\text{M} = \text{Ni}, \text{V}; n = 2, 3$) used for the calculations are based on the experimental structures of $\text{Ni}(\text{H}_2\text{O})_6(\text{NO}_3)_2$,²³ $\text{NiCl}_2(\text{H}_2\text{O})_4$,²⁴ and $\text{Cs}_4\text{V}(\text{H}_2\text{O})_6(\text{SO}_4)_2 \cdot 6\text{H}_2\text{O}$,²⁵ $\text{Cs}_3\text{VCl}_6 \cdot 4\text{H}_2\text{O}$ ²⁶ with metal–oxygen distances of 2.06 and 1.97 Å for Ni–O and V–O, respectively. The model geometry and coordinate system used in the calculations are shown in Figure 2. These bond lengths are varied to obtain the potential energy surfaces shown in the following. The ligands are defined by O–H distances of 1.04 Å and H–O–H angles of 104.5°. Their structure and the orientation of the H_2O plane are not varied for our calculations.

The electronic configuration of $[\text{Ni}(\text{H}_2\text{O})_6]^{2+}$ in its ${}^3\text{A}_{2g}$ ground state is $(3d_{xy})^2(3d_{xz})^2(3d_{yz})^2(3d_{x^2-y^2})^1(3d_{z^2})^1$, corresponding to $(t_{2g})^6(e_g)^2$ in the O_h point group, whereas the ${}^3\text{T}_{1g}$ electronic ground state of $[\text{V}(\text{H}_2\text{O})_6]^{3+}$ is given by $(3d_{xy})^2(3d_{xz})^2(3d_{yz})^2(3d_{x^2-y^2})^0(3d_{z^2})^0$, corresponding to $(t_{2g})^2(e_g)^0$ in the O_h point group. To analyze the spectroscopy of $[\text{M}(\text{H}_2\text{O})_6]^{n+}$, the low-energy triplet excited states generated by the single and double excitations within the 3d orbitals manifold have been calculated. Averaged CASSCF calculations in which eight electrons ($\text{M} = \text{Ni}^{2+}$) or two electrons ($\text{M} = \text{V}^{3+}$) have been correlated in 13 active orbitals (the five 3d orbitals of the metal centers, the 3d of correlation, and some diffuse orbitals delocalized over the oxygen atoms and the metal center) have been performed in order to generate the zero-order wave functions used as references in subsequent CASPT2 calculations that include the dynamical correlation effects. This active space was chosen to be identical for both title complexes in order to

provide calculated spectroscopic properties that can be compared. The correlated calculations have been driven in D_{2h} symmetry, and a level shift correction of 0.4 has been applied in the case of the nickel complex to eliminate intruder states.^{27,28} Spin–orbit effects are not included in the present calculations. The spin–orbit splitting of the triplet states in first-row transition metal complexes does not exceed a few hundreds of wavenumbers, a small effect compared to the nonadiabatic coupling on the order of thousands of wavenumbers, which is of interest here.

Let us note that the CASPT2 method, which is essentially monoconfigurational, should be used with care in situations of states mixing. In such cases, the zero-order CASSCF wave function has to correctly describe this mixing in order to avoid erroneous results from the perturbational treatment. This is a potentially serious problem in the nickel complex. However, the stability of the CASPT2 calculation is assured by a nearly constant reference weight ω of approximately 0.70 in the case of the vanadium complex and 0.76 in the case of the nickel compound for all electronic states and geometry variations investigated here.

On the basis of the experimental spectroscopic data, the totally symmetric average elongation of the M–O bonds along the normal coordinate ΔQ_{a1g} has been retained as the most important mode of deformation of the molecules in the crystal-field triplet excited states investigated here. The origin of the ΔQ_{a1g} axis is set at the ground-state equilibrium geometry. The PEC associated to these low-lying triplet states are calculated as a function of this coordinate at the CASSCF and CASPT2 levels. Harmonic frequencies and the positions of the potential minima along the abscissa, denoted as $\Delta Q_{a1g\text{min}}$, were obtained from these calculations as summarized in Tables 1 and 2. We note that the rather large energy separation between the ${}^3\text{T}_{1g}({}^3\text{F})$ and ${}^3\text{T}_{1g}({}^3\text{P})$ states of $[\text{Ni}(\text{H}_2\text{O})_6]^{2+}$ complex justifies a posteriori the computational method that describes the mixing at the zero order only (CASSCF).

The basis sets, which are of generally contracted atomic natural orbital (ANO) type, are the following:²⁹ for the nickel and vanadium atoms, a (17s, 12p, 9d, 4f) set contracted to [5s, 4p, 3d]; for the oxygen atoms, a (10s, 6p, 3d) set contracted to [3s, 2p, 1d]; and for the hydrogen atoms, a (7s, 3p) set contracted to [2s, 1p].

The calculations have been performed with the program system MOLCAS4.1.³⁰

Computational Results and Discussion

Crystal Field States. We present crystal field energy level diagrams to illustrate the electronic states important for the following discussion. The Tanabe–Sugano diagrams for $[\text{V}(\text{H}_2\text{O})_6]^{3+}$ and $[\text{Ni}(\text{H}_2\text{O})_6]^{2+}$ are given in parts a and b of Figure 3, respectively. The coupling between the ${}^3\text{T}_{1g}$ states is obvious for both configurations, and the d^8 diagram shows a prominent avoided crossing near the Dq range for the H_2O ligand. The corresponding effect is also visible in the d^2 diagram, where the two ${}^3\text{T}_{1g}$ states are closest at $Dq = 0$, far from the region of the H_2O ligand.

- (21) Wilson, R. B.; Solomon, E. I. *Inorg. Chem.* **1978**, *17*, 1729.
 (22) Güdel, H. U.; Snellgrove, T. R. *Inorg. Chem.* **1978**, *17*, 1617.
 (23) Bigoli, F.; Braibanti, A.; Tiripicchio, A.; Tiripicchio, C. *Acta Crystallogr.* **1971**, *B27*, 1427.
 (24) Mizuno, J. J. *Phys. Soc. Jpn.* **1961**, *16*, 1574.
 (25) Beattie, J. K.; Best, S. P.; Skelton, B. W.; White, A. H. *J. Chem. Soc., Dalton Trans.* **1981**, 2105.
 (26) McCarthy, P. J.; Lauffenburger, J. C.; Schreiner, M. M.; Rohrer, D. C. *Inorg. Chem.* **1981**, *20*, 1571.

- (27) Roos, B. O.; Anderson, K.; Fülscher, M. P.; Serrano-Andres, L.; Pierloot, K.; Merchan, M.; Molina, V. *THEOCHEM* **1996**, *388*, 257.
 (28) Roos, B. O.; Anderson, K. *Chem. Phys. Lett.* **1995**, *245*, 215.
 (29) Pierloot, K.; Dumez, B.; Widmark, P. O.; Roos, B. O. *Theor. Chim. Acta* **1995**, *90*, 87.
 (30) Andersson, K.; Blomberg, M. R. A.; Fülscher, M. P.; Karlström, G.; Lindh, R.; Malmqvist, P.; Neogrády, P.; Olsen, J.; Roos, B. O.; Sadlej, A. J.; Schütz, M.; Seijo, L.; Serrano-Andrés, L.; Siegbahn, P. E. M.; Widmark, P. O. *MOLCAS*, 4.1 ed.; Lund University: Lund, Sweden, 1997.

Table 1. Calculated Equilibrium Distances ΔQ_{a1gmin} , Minimum Energies E_{min} , and Vibrational Frequencies $\hbar\omega$ for the Triplet Crystal Field States of $[V(H_2O)_6]^{3+}$ (Experimental Values Are Given in Parentheses)

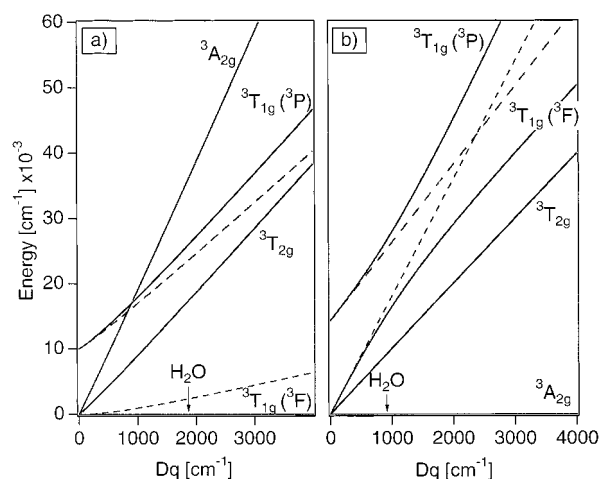
electronic state	CASSCF			CASPT2		
	ΔQ_{a1gmin} (Å)	E_{min} (cm ⁻¹)	$\hbar\omega$ (cm ⁻¹)	ΔQ_{a1gmin} (Å)	E_{min} (cm ⁻¹)	$\hbar\omega$ (cm ⁻¹)
$^3T_{1g}(^3F)$	0	0	124	0	0	253 (530 ^b)
$^3T_{2g}$	-0.71	9660	227	0.23	9830 (13400 ^a)	320
$^3T_{1g}(^3P)$	-0.73	23680	222	0.19	19930 (20700 ^a)	318

^a Estimated from Figure 1a. ^b From ref 15.

Table 2. Calculated Equilibrium Distances ΔQ_{a1gmin} , Minimum Energies E_{min} , and Vibrational Frequencies $\hbar\omega$ for the Triplet Crystal Field States of $[Ni(H_2O)_6]^{2+}$ (Experimental Values Are Given in Parentheses)

electronic state	CASSCF			CASPT2		
	ΔQ_{a1gmin} (Å)	E_{min} (cm ⁻¹)	$\hbar\omega$ (cm ⁻¹)	ΔQ_{a1gmin} (Å)	E_{min} (cm ⁻¹)	$\hbar\omega$ (cm ⁻¹)
$^3A_{2g}$	0	0	318	0	0	300 (397 ^b)
$^3T_{2g}$	0.12	5678	346	0.17	7039 (6600 ^a)	332
$^3T_{1g}(^3F)$	0.17	8308	356	0.23	9724 (11300 ^a)	343 (350 ^c)
$^3T_{1g}(^3P)$	0.14	24850	350	0.18	23703 (23000 ^a)	337

^a Estimated from Figure 1a. ^b Raman, 77 K, this work. ^c Reference 16.

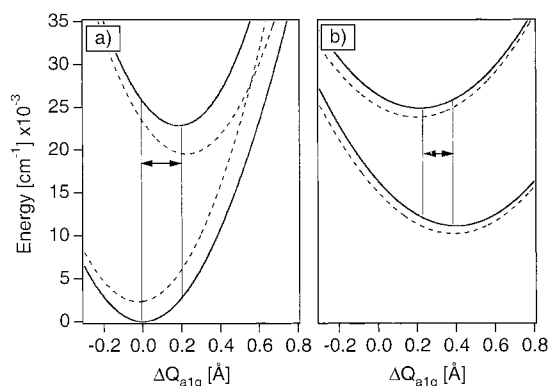
**Figure 3.** Tanabe–Sugano diagram for (a) $[V(H_2O)_6]^{3+}$ and (b) $[Ni(H_2O)_6]^{2+}$. The diagrams include only the triplet states discussed in this study. The position of the H_2O ligand for both complexes is indicated on the Dq axis. The broken lines give the energies of the $^3T_{1g}$ states if the off-diagonal matrix element coupling these states is set to zero.

The electronic energies of the coupled states are calculated as the eigenvalues of the weak-field energy matrix:³¹

$$\begin{vmatrix} -6Dq - E(^3T_{1g}(^3F)) & 4Dq \\ 4Dq & 15B - E(^3T_{1g}(^3P)) \end{vmatrix} = 0 \quad (1)$$

The dotted lines in Figure 3 denote the diagonal elements of this matrix. The coupling constant between the states is $4Dq$, and the solid lines denote the energies of the $^3T_{1g}$ crystal field states. We note that the corresponding strong-field matrix leads to the same eigenvalues as eq 1.³¹ Numerical values for pairs of parameters Dq , B are 910 cm⁻¹, 950 cm⁻¹ and 1860 cm⁻¹, 665 cm⁻¹ ³² for $[Ni(H_2O)_6]^{2+}$ and $[V(H_2O)_6]^{3+}$, respectively, as indicated on the abscissa of Figure 3.

Crystal field energies for all triplet states define the point of each excited state potential energy surface directly above the ground-state equilibrium geometry. Both diabatic and adiabatic potentials for the two $^3T_{1g}$ states can be obtained by adding

**Figure 4.** Schematic potential energy surfaces for the $^3T_{1g}$ states of (a) $[V(H_2O)_6]^{3+}$ and (b) $[Ni(H_2O)_6]^{2+}$. Solid and broken lines denote adiabatic and diabatic potentials, respectively.

harmonic terms in ΔQ_{a1g} to the diagonal elements of eq 1.³ These surfaces are shown as dotted and solid lines in Figure 4. The offset of the minima along the abscissa is qualitative and increases with the number of electrons in the σ -antibonding e_g orbitals of the predominant electronic configurations of the two coupled states. We expect the ground-state potential energy minimum for the vanadium(III) complex at a lower value of ΔQ_{a1g} than for the excited state, which arises from the $(t_{2g})^1(e_g)^1$ configuration, with a higher e_g σ -antibonding electron density than the ground state (Figure 4a). The adiabatic potentials are calculated with the coupling constant of $4Dq$ given in eq 1 and the experimental vanadium-water stretching frequency of 530 cm⁻¹.¹⁵ These adiabatic potentials retain the essential aspects of the harmonic diabatic surfaces: the V–O bond length is shorter in the $^3T_{1g}$ ground state than in the excited state with $^3T_{1g}$ symmetry. The minimum of the adiabatic potential curve in Figure 4a is lower in energy by 2330 cm⁻¹ than the minimum of the diabatic curve. The vertical lines denote the positions of the minima of the adiabatic potentials. They are slightly closer to each other than the minima of the harmonic potentials, which are separated by 0.2 Å. The separation remains large, as shown by the horizontal double arrow in Figure 4a and leads to the broad $^3T_{1g}(^3F) \rightarrow ^3T_{1g}(^3P)$ absorption band.

The situation is different for the nickel complex, as shown in Figure 4b. The diabatic potentials are calculated with a vibrational frequency of 350 cm⁻¹, determined from the resolved spectra in Figure 1b and their minima are separated by 0.2 Å, the same value used for the corresponding states in Figure 4a.

(31) König, E. *Struct. Bond.* **1971**, 9, 175.

(32) Figgis, B. N. *Introduction to Ligand Fields*; Interscience: New York, 1966.

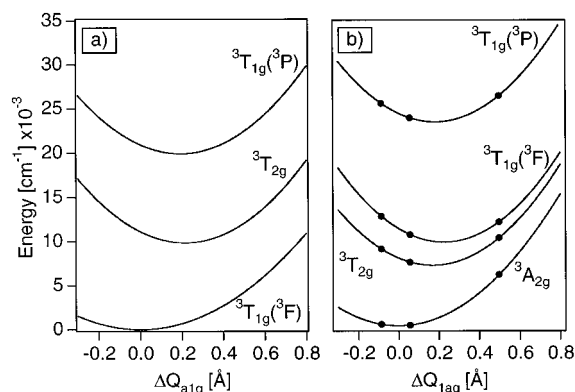


Figure 5. CASPT2 potentials for (a) $[\text{V}(\text{H}_2\text{O})_6]^{3+}$ and (b) $[\text{Ni}(\text{H}_2\text{O})_6]^{2+}$. Dots indicate molecular geometries for which configuration-state functions are given in Table 3.

The ${}^3\text{T}_{1g}({}^3\text{F})$ excited-state arises from the $(t_{2g})^4(e_g)^4$ configuration (in the formalism used for eq 1) and its diabatic potential has a larger offset along the abscissa than the higher energy ${}^3\text{T}_{1g}({}^3\text{P})$ excited state, which arises from the $(t_{2g})^5(e_g)^3$ configuration with less e_g σ -antibonding electron density. We illustrate this difference by the position of the minima of the diabatic potential along Q . The minimum of the state arising from $(t_{2g})^5(e_g)^3$ is at 0.2 Å and the minimum of the state arising from $(t_{2g})^4(e_g)^4$ is at 0.4 Å, assuming an identical increase along Q for each electron placed into the σ -antibonding orbitals. The character of the adiabatic potentials is strongly mixed and varies along Q . This mixing leads to potential minima that are closer together than for the corresponding states in Figure 4a, as illustrated by the vertical lines and the shorter double arrow in Figure 4b. These similar potential curves rationalize the comparable bandwidths observed for the two transitions to ${}^3\text{T}_{1g}$ excited states shown in Figure 1a. Crystal field calculations give only a qualitative description of this variation, because they strongly depend on the choices made for the parameters Dq , B and C ^{13,33,34} and only d electronic configurations are considered. The most important aspect of the qualitative ${}^3\text{T}_{1g}$ potentials in Figure 4b is that they no longer strictly reflect the different electronic configurations of the two diabatic states. In analogy to the electronic energies in Figure 3, there are several different ways of defining diabatic potentials that lead to identical adiabatic potential surfaces. In the crystal field approach, the two traditional ways are the weak-field and strong-field formalisms. This problem has been discussed in detail in the literature.³⁵

The qualitative PEC in Figure 4 show that coupled potentials cross very far from the Franck–Condon region. We therefore use the adiabatic approximation to calculate absorption spectra throughout the following. To obtain a more quantitative picture of the potentials illustrated in Figure 4a,b, ab initio calculations presented in the following section have been performed using the CASSCF/CASPT2 approach.

Potentials Associated to the Triplet Crystal Field States of $[\text{V}(\text{H}_2\text{O})_6]^{3+}$. The CASPT2 PEC calculated as a function of ΔQ_{a1g} and associated to the ${}^3\text{T}_{1g}({}^3\text{F})$ electronic ground state and to the low-lying ${}^3\text{T}_{1g}({}^3\text{P})$ and ${}^3\text{T}_{2g}$ excited states of $[\text{V}(\text{H}_2\text{O})_6]^{3+}$ are represented in Figure 5a. The corresponding calculated vibrational frequencies, minimum energies and equilibrium M–O distances are reported in Table 1. Values reported in Table

1 and in the figure are obtained from one representative of the ${}^3\text{B}_{1g}$, ${}^3\text{B}_{2g}$, ${}^3\text{B}_{3g}$ states arising from each ${}^3\text{T}_{1g,2g}$ state in the D_{2h} symmetry of our model shown in Figure 2.

The potential minima of the ${}^3\text{T}_{2g}$ and ${}^3\text{T}_{1g}({}^3\text{P})$ excited states are shifted along ΔQ_{a1g} by 0.22 and 0.19 Å, respectively, at the CASPT2 level. As expected from the schematic picture in Figure 4a, the minima of the ${}^3\text{T}_{1g}$ ground and excited states do not coincide. Obviously, CASSCF calculations give only a qualitative picture of the potentials and associated properties, as illustrated by the values listed in Table 1. For instance, the minimum of the ground state PEC is obtained at an unphysically large value of the normal coordinate from the CASSCF calculations and at a much more reasonable position with respect to experimental bond lengths at the CASPT2 level. This is due to the dynamical correlation effects (not included at the CASSCF level), which are very large in transition metal complexes. These correlation effects arise from the multiple excitation of the CASSCF inactive electrons and in general vary for different electronic states and as a function of the normal coordinate Q . As a consequence, the shape and relative positions of the CASPT2 potentials generally differ significantly from those obtained at the CASSCF level, but different electronic states are not affected to the same amount.

The lowest singlet excited state is calculated at 9270 and 9890 cm^{-1} with CASSCF and CASPT2, respectively, very close to the corresponding sharp experimental absorption band observed at 10200 cm^{-1} for $[\text{V}(\text{H}_2\text{O})_6]^{3+}$ doped into a cesium aluminum alum lattice.¹⁵ We have recently measured the highest-energy luminescence transition for $[\text{V}(\text{D}_2\text{O})_6]^{3+}$ at 10234 cm^{-1} . This good agreement between experimental and calculated energies of the lowest spin-flip transition further corroborates the validity of our model calculations.

Potentials Associated to the Crystal Field Triplet States of $[\text{Ni}(\text{H}_2\text{O})_6]^{2+}$. The CASPT2 PEC calculated as a function of ΔQ_{a1g} and associated to the ${}^3\text{A}_{2g}$ electronic ground state and to the low-lying ${}^3\text{T}_{1g}({}^3\text{F})$, ${}^3\text{T}_{1g}({}^3\text{P})$, and ${}^3\text{T}_{2g}$ states of $[\text{Ni}(\text{H}_2\text{O})_6]^{2+}$ are represented in Figure 5b. The corresponding calculated vibrational frequencies, minimum energies and equilibrium Ni–O bond length changes are summarized in Table 2. Values reported in this Table are obtained from one representative of the ${}^3\text{B}_{1g}$, ${}^3\text{B}_{2g}$, ${}^3\text{B}_{3g}$ states arising from each ${}^3\text{T}_{1g,2g}$ state in the D_{2h} symmetry of the model structure shown in Figure 2.

The resolved vibronic structure of the ${}^3\text{T}_{2g}$ band of $[\text{Ni}(\text{H}_2\text{O})_6]^{2+}$ in Figure 1b allows us to estimate the position of the minimum $\Delta Q_{a1g\text{min}}$ of this excited state PEC with respect to the ground state equilibrium geometry. The intensities of the first two members of the progression in the totally symmetric M–H₂O stretching mode are given as I_0 and I_1 in Figure 1b. The ratio I_1/I_0 is not significantly different for the deuterated complex, and we determine a value of 2.2 from the spectra. The value of $\Delta Q_{a1g\text{min}}$ is given as^{1,2}

$$\Delta Q_{a1g\text{min}} = \frac{8.2118 \sqrt{\frac{I_1}{I_0}}}{\sqrt{\hbar\omega m}} \quad (2)$$

where $\hbar\omega$ denotes the vibrational frequency of the excited state, determined as 350 cm^{-1} from Figure 1b, and m is the mass of the ligand, 18 g/mol. We calculate a value of 0.15 Å from eq 2, in excellent agreement with the value of 0.16 Å from the CASPT2 results in Table 2, again illustrating the good quality of the calculations. A similar analysis for the other excited states

(33) Ballhausen, C. J. *Introduction to Ligand Field Theory*; McGraw-Hill: New York, 1962.

(34) Tanabe, Y.; Moriya, T.; Sugano, S. *Phys. Rev. Lett.* **1965**, *15*, 1023.

(35) Talaga, D. S.; Zink, J. I. *J. Phys. Chem.* **1996**, *100*, 8712–8721.

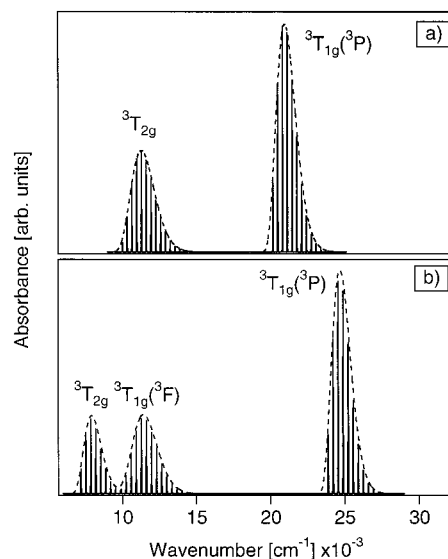
Table 3. CASSCF Weights (%) of the Configuration-State Functions for the Triplet Excited States of $[\text{Ni}(\text{H}_2\text{O})_6]^{2+}$

ΔQ_{a1g} (Å)	${}^3T_{2g}$		${}^3T_{1g}({}^3F)$		${}^3T_{1g}({}^3P)$	
	$(t_{2g})^5(e_g)^3$	$(t_{2g})^4(e_g)^4$	$(t_{2g})^5(e_g)^3$	$(t_{2g})^4(e_g)^4$	$(t_{2g})^4(e_g)^4$	$(t_{2g})^5(e_g)^3$
0	97	70	26	27	73	
0.146	97	72	25	25	63	
0.588	97	76	21	21	67	

is not possible because the absorption bands do not show resolved structure.

The CASPT2 vibrational energies and minima of the PEC are in the range of the experimental values. Recent calculated frequencies reported in the literature for the ground state of several chromium(III) halide complexes deviate by up to 30% from the experimental frequencies measured for single crystals,^{36,37} comparable to the differences we report in Tables 1 and 2. Another recent study on manganese(IV) doped into a fluoride lattice reports discrepancies of up to 20% between calculated and experimental ground-state frequencies.³⁸ These studies involve isotropic metal–ligand π bonds, in contrast to the present work, where anisotropic π bonding occurs and is represented by the model structure in Figure 2. We examine only the variation of the metal–oxygen bond lengths and neglect the effects that an optimization of the orientation of the plane of each water ligand could have on vibrational frequencies in all electronic states of interest. Some of the literature studies include the crystal environment in the calculations, a second aspect that was neglected in the present study, but could also influence vibrational frequencies and transition energies. In view of these simplifications, the agreement between calculated and observed frequencies is satisfactory. Excited-state frequencies are usually not reported in the literature. The higher frequencies calculated for some excited states are counterintuitive, but the difference is within the variation between experimental and calculated values for the ground state.

In contrast to the vanadium complex, where the PEC calculated for the two ${}^3T_{1g}$ states have their minima close to the values expected without considering coupling between states, we observe here important effects due to mixing between these two electronic states as a function of the totally symmetric normal coordinate ΔQ_{a1g} . This is illustrated by the CASSCF weights of the configuration-state functions reported in Table 3. For instance, we observe an increase of the $(t_{2g})^4(e_g)^4$ configuration from 70 to 76% in the ${}^3T_{1g}({}^3F)$ state with the Ni–O bond elongation over the range given by the solid circles in Figure 5b. Even though this mixing occurs far from the crossing region, it will cause significant spectroscopic effects, illustrated by the relative positions of the potential minima associated to the two ${}^3T_{1g}$ states, which are within 0.06 Å despite their different electronic character. For comparison, in the vanadium complex, these states remain nearly pure (89% $(t_{2g})^2(e_g)^0$ for ${}^3T_{1g}({}^3F)$, 92% $(t_{2g})^1(e_g)^1$ for ${}^3T_{1g}({}^3P)$), and their character varies by less than 3% over the same range of ΔQ_{a1g} , leading to minima separated by 0.19 Å, a much larger value than for the nickel complex. Finally, we note that the character of the ${}^3T_{2g}$ state for the nickel complex does not vary at all at the geometries in Table 3, again confirming the relevance of the state mixing calculated for the ${}^3T_{1g}$ excited states.

**Figure 6.** Absorption spectra for the spin-allowed transitions calculated from the CASPT2 potential curves for (a) $[\text{V}(\text{H}_2\text{O})_6]^{3+}$ and (b) $[\text{Ni}(\text{H}_2\text{O})_6]^{2+}$.

Calculated Absorption Spectra. The spectroscopic effects induced by coupling between the ${}^3T_{1g}$ states are illustrated by the calculated spectra in Figure 6, which were obtained from the CASPT2 potentials in Figure 5. All absorption spectra were calculated using equal transition dipoles for each band. This assumption is justified by the experimental spectra of the nickel(II) complex, which do not show an unusually weak band for the transition corresponding predominantly to the two-electron excitation. Even in some vanadium(III) complexes, whose spectra contain an unusually weak band for the formal two-electron excitation from the ${}^3T_{1g}$ ground state to the ${}^3A_{2g}$ excited state, the experimental intensity of this band has been shown to be higher by orders of magnitude than estimated from the mixing coefficients.³⁹ Other factors, such as the efficiency of various ungerade parity enabling modes, appear to have a more important influence than the mixing coefficients. The absorption spectrum is calculated as^{1,2}

$$I_{\text{abs}}(\omega) = \omega \int_{-\infty}^{\infty} e^{i\omega t} \langle \phi | \phi(t) \rangle e^{-\Gamma^2 t^2 + (iE_{00}/\hbar)t} dt \quad (3)$$

The linear frequency factor ω causes the different relative intensities of the calculated bands in Figure 6. The autocorrelation functions and Fourier transforms were calculated as described in detail previously.³ The origins E_{00} of the calculated bands for $[\text{V}(\text{H}_2\text{O})_6]^{3+}$ are at 9830 and 19 930 cm^{-1} and compare well to the origin energies estimated from the experimental spectra at 13 400 and 20 700 cm^{-1} , respectively. The calculated bands are narrower by 25–50% than the experimental bands. The most likely reasons for this discrepancy are effects neglected in our model, such as Jahn–Teller distortions, and excited-state splittings due to low site symmetry,¹⁸ energy differences between vibronic origins, which give rise to the main observed intensity, and spin–orbit coupling. All these effects lead to experimental bands that are larger than the calculations based on the PECs in Figure 5. The overall agreement between experiment and calculations is satisfactory.

Figure 6b shows the calculated absorption spectrum with all spin-allowed transitions of the nickel complex. As for the

(36) Bellafrouh, K.; Daul, C.; Güdel, H.-U.; Gilardoni, F.; Weber, J. *Theor. Chim. Acta* **1995**, *91*, 215.

(37) Gilardoni, F.; Weber, J.; Bellafrouh, K.; Daul, C.; Güdel, H.-U. *J. Chem. Phys.* **1996**, *104*, 7624.

(38) Seijo, L.; Barandiarán, Z.; McClure, D. S. *Int. J. Quantum Chem.* **2000**, *80*, 623.

(39) Ballhausen, C. J. *Z. Phys. Chem.* **1958**, *17*, 246.

vanadium complex, the spectrum is obtained from the CASPT2 potential curves using identical transition dipoles for each band. The calculated electronic origins of the three bands are at 7039, 9724, and 23 703 cm^{-1} , and the calculated spectrum shows a large energy gap of 13 280 cm^{-1} between the two ${}^3\text{T}_{1g}$ band maxima. This energy difference is larger by almost a factor of 2 than the energy difference between the ground state and the lowest energy excited state, where the band maximum is calculated at 7910 cm^{-1} . The mixing of the ${}^3\text{T}_{1g}$ states contributes significantly to their large energy separation, illustrated by the schematic potential energy surfaces in Figure 4b. The calculations rationalize the experimental observation of very similar bandwidths for the two ${}^3\text{T}_{1g}$ bands in many octahedral nickel(II) complexes, even though the two states formally arise from different electronic configurations.

The comparison of the two calculated spectra in Figure 6 shows that the first band is at lower energy for the divalent nickel complex than for the trivalent vanadium complex, in agreement with the higher 10Dq value expected for the vanadium ion with its higher charge. The calculated spectra also confirm the experimental observation that the transition to the ${}^3\text{T}_{1g}({}^3\text{P})$ excited state occurs at higher energy in the nickel complex than in its vanadium analogue. This is due to the higher energy of the atomic ${}^3\text{P}$ parent term in the nickel complex and to the steeper slope of the ${}^3\text{T}_{1g}({}^3\text{P})$ state as a function of Dq, as illustrated in Figure 3b. The steeper slope is a consequence of the significant 27% contribution of the electronic configuration with two additional electrons in the e_g orbitals to ${}^3\text{T}_{1g}({}^3\text{P})$, a direct energetic manifestation of the configuration mixing in the nickel complex.

The ab initio calculations show that the potential minima of the ${}^3\text{T}_{1g}({}^3\text{F})$ and ${}^3\text{T}_{1g}({}^3\text{P})$ states in the nickel complex are at very similar positions along the ΔQ_{a1g} axis, as illustrated in Table 2. This model study reveals that even states separated by

a large energy difference can interact in ways that affect the experimental absorption spectrum.

Conclusion

Our combined experimental and theoretical study focuses on the effects of coupling between electronic states in $[\text{V}(\text{H}_2\text{O})_6]^{3+}$ and $[\text{Ni}(\text{H}_2\text{O})_6]^{2+}$, model complexes with the d^2 and d^8 electronic configurations, respectively. The main qualitative trends are illustrated by a simple crystal field analysis. Quantitative spectroscopic properties have been extracted from CASSCF/CASPT2 potentials associated to the low-lying triplet states and calculated as a function of a single normal coordinate, the totally symmetric M–H₂O stretching mode. The theoretical approach has enabled us to describe and to analyze the significant mixing between the two ${}^3\text{T}_{1g}$ states in $[\text{Ni}(\text{H}_2\text{O})_6]^{2+}$. This strong interaction characterizing the nickel compound leads to potentials with minima at almost the same position along the normal coordinate, in contrast to the vanadium analogue, where they are separated by approximately 0.2 Å. The interaction between states is an important reason for the observation of two ${}^3\text{T}_{1g}$ bands with nearly identical widths in the experimental spectra of many octahedral nickel complexes.

Acknowledgment. This work was made possible by grants and fellowships (to J.L.-H. and G.B.) from the Natural Sciences and Engineering Research Council (Canada) and by a visiting faculty fellowship (to C.R.) from the Ministère des relations internationales (Province of Quebec) and the Ministère des affaires étrangères (France). We thank Myriam Triest (Université de Montréal) for helpful discussions. The calculations have been carried out either at the IDRIS (Orsay, France) through a grant of computer time from the Conseil Scientifique or at the LCQS (Strasbourg, France).

IC0010860